Research Square

Preprints are preliminary reports that have not undergone peer review.
They should not be considered conclusive, used to inform clinical practice,
or referenced by the media as validated information.

Raw jujube stone and raw hawthorn stone particles as green adsorbents for the adsorption of different organic dyes

Seyed Hossein Mousavi

shom7@yahoo.com

University of Guilan

Susan Jafari

University of Guilan

Sahar Hanifehpour

University of Guilan

Hadi Fallah Moafi

University of Guilan

Research Article

Keywords: Raw jujube stone, Raw hawthorn stone, Adsorption, Green adsorbent, Organic dyes

Posted Date: November 21st, 2026

DOI: https://doi.org/10.21203/rs.3.rs-11231979/v1

License: This work is licensed under a Creative Commons Attribution 4.0 International License.
Read Full License

Additional Declarations: No competing interests reported.

Raw jujube stone and raw hawthorn stone particles as green adsorbents for the adsorption of different organic dyes

Seyed Hossein Mousavi [a,*], Susan Jafari [a], Sahar Hanifehpour [a], Hadi Fallah Moafi [a]

[a] Department of Inorganic Chemistry, Faculty of Chemistry, University of Guilan, Rasht, Iran

* E-mail of corresponding authors: shom7@yahoo.com (S.H. Mousavi)

Abstract

In this work, the raw jujube stone particles (RJSP) and the raw hawthorn stone particles (RHSP) as efficient natural and green adsorbents were used for the adsorption of methylene blue (MB), malachite green (MG), crystal violet (CV), and disperse red 1 (DR1) dyes. The functional groups, morphology, particle size, surface area, and pore size of RJSP and RHSP were determined using FT-IR, BET, FESEM, TEM, and EDX. The green adsorbents RJSP and RHSP showed high efficiency in the adsorption of MB, MG, CV, and DR1 dyes and showed comparable performance to other reported adsorbents. According to the results, the adsorption of MB, MG, CV, and DR1 dyes onto RJSP and RHSP follows the Freundlich isotherm, while the kinetics are well described by the pseudo-second-order model. Also, according to the Langmuir isotherm, RJSP exhibited maximum adsorption capacities (Q_m) of 145, 124, 114, and 98 mg/g for MB, MG, CV, and DR1, respectively, while RHSP showed adsorption capacities of 84, 111, 102, and 94 mg/g. In addition, thermodynamic parameters confirm that the adsorption of MB, MG, CV, and DR1 dyes is exothermic on RJSP and endothermic on RHSP. Finally, the RJSP and RHSP can be used as affordable, environmentally friendly, and effective natural adsorbents for the removal of various industrial dyes.

Keywords: Raw jujube stone; Raw hawthorn stone; Adsorption; Green adsorbent; Organic dyes.

1. Introduction

Adsorbents and adsorption methods are important research topics in environmental science. Water pollutants include organic compounds, ions and Heavy metals, dyes, drugs, and others [1–5]. Among water pollutants, dyes play a key role in water pollution because of their destructive impacts on humans and the environment. Textile industries are among the most important sources of environmental pollution through the release of dyes due to the use of various chemicals [6–8]. Therefore, effective treatment of dye-contaminated wastewater is essential for protecting the aquatic environment.

In recent years, for the removal of dyes, various methods such as membrane filtration, biological treatments, ultrafiltration, photocatalytic, sonochemical, and electrochemical degradation, and adsorption have been used [9–16]. Among these, adsorption method is simpler and cheaper than other dye removal techniques and has proven effective [17,18]. The main disadvantage of synthetic adsorbents is the cost of obtaining raw materials, but the use of natural adsorbents makes this method a simpler and more economical way to remove dyes.

Many green adsorbents, including banana peel, sawdust, rice bran, pine bark, soybean hulls, peanut shells, olive kernels, orange peels, date stones, almond shells, etc., have been widely investigated for the adsorption of dyes due to their abundant availability and low cost [19–28]. On an industrial scale, the use of natural and green adsorbents is more cost-effective and valuable than synthetic adsorbents. Jujube stone and hawthorn stone are agricultural wastes that are available in large quantities and have no economic value. Therefore, they can serve as suitable green adsorbents for the removal of dyes.

The present work aimed to investigate the adsorption of organic dyes by raw jujube stone particles (RJSP) and the raw hawthorn stone particles (RHSP) as green adsorbents through batch adsorption experiments while evaluating the influence of various experimental parameters. The functional groups, morphology, particle size, surface area, and pore size of RJSP and RHSP were determined using FT-IR, BET, FESEM, TEM, and EDX analysis. To better understand the adsorption mechanism, isotherm, kinetic, and thermodynamic analyses were studied.

2. Experimental section

2.1. Materials and equipment

The jujube and hawthorn were prepared in Rasht city, Guilan province, Iran. Methylene blue (MB), malachite green (MG), crystal violet (CV), disperse red 1 (DR1), sodium hydroxide (NaOH), hydrochloric acid (HCl), methanol, ethanol, and acetonitrile were obtained from Sigma-Aldrich. All experiments were conducted using deionized water. The FT-IR, BET, FESEM, TEM and EDX analyses were used to determine the functional groups, morphology, particle size and surface area of RJSP and RHSP. The model of the devices used is given in the Supplementary information (SI).

2.2. The preparation of RJSP and RHSP green adsorbents

The jujube stone and hawthorn stone were obtained from agricultural waste in Rasht, Guilan province, Iran. First, the raw jujube stone (RJSP) and raw hawthorn stone (RHSP) were thoroughly rinsed using deionized water and subsequently oven-dried at 100 °C for 6 h. The dried RJSP and RHSP were then ground several times and sieved to obtain uniform particle size. The RJSP and RHSP were used in the experiments without chemical modification.

2.3. Batch adsorption experiment

To better understand adsorption behavior, the RJSP and RHSP were investigated in batch systems using MB, MG, CV, and DR1 as representative dyes. Adsorption tests were conducted using 0.015 g of RJSP and RHSP in 10 mL of each dye solution (MB, MG, CV, and DR1) each prepared at 50 mg/L. To evaluate the adsorption process, the effects of pH (3–12), contact time (2–20 min), adsorbent dosage (0.003–0.030 g), operating temperature (25–85 °C), and initial dye concentration (50–200 mg/L) were studied over their respective ranges. Residual dye concentrations were measured at the maximum wavelengths (λ_{max}) of 660, 610, 590, and 517 nm for MB, MG, CV, and DR1, respectively. To ensure reliability, all adsorption tests were performed three times, and the data were reported as mean values. In addition, isotherm, kinetic, and thermodynamic analyses were performed to better interpret the adsorption mechanism (Table S1, Supplementary information).

3. Results and discussion

3.1. Characterization

3.1.1. FT-IR characterization

Fig.1 represents a comparison of the FT-IR spectra recorded for RJSP, RHSP, dyes-adsorbed RJSP, and dyes-adsorbed RHSP. As shown in Fig.1 (a), the absorption band at 896 cm^{-1} in the FT-IR spectrum of RJSP is attributed to C–H bending vibrations. The bands observed at 1265 cm^{-1} and 1037 cm^{-1} correspond to C–O stretching vibrations related to carboxylic acid and alcohol groups. The Absorption bands at 1463 and 1325 cm^{-1} were assigned to the C–O vibrations of methoxy groups in lignin. Peaks appearing at 1738 and 1656 cm^{-1} were attributed to the C=O stretching vibration of carboxylic acid groups and the aromatic C=C stretching

vibration of lignin in the jujube stone, respectively. The absorption band at 2927 cm^{-1} can be assigned to aliphatic C–H asymmetric stretching vibrations associated with the biomass components (hemicellulose, cellulose, and lignin). Also, a wide absorption band at 3421 cm^{-1} is attributed to the stretching vibration of hydroxyl (OH) groups [29–32].

The absorption band appearing at 895 cm^{-1} in the RHSP FT-IR spectrum (Fig.1 (b)) is associated with C–H bending vibrations. The peaks at 1266 and 1045 cm^{-1} are attributed to the C–O stretching vibrations associated with carboxylic acid and alcohol groups. Characteristic absorption bands at 1649 cm^{-1} and 1737 cm^{-1} suggest the presence of amide groups and –C=O from carboxyl or ester groups in the RJSP, respectively. The band observed at 2928 cm^{-1} is characteristic of the aliphatic C-H stretching vibration in the RJSP. Also, the broad band at 3420 cm^{-1} corresponds to the O-H stretching vibration of hydroxyl groups. This functional group confirms the presence of alcoholic or phenolic -OH groups in the hawthorn stone [33–36].

Also, the FT-IR spectra of dyes-adsorbed RJSP and dyes-adsorbed RHSP are shown in Fig.1 (c) and Fig.1 (d). After dye adsorption, the characteristic peak intensities of RJSP and RHSP decreased, confirming that the dye molecules interacted with the surface functional groups of the RJSP and RHSP.

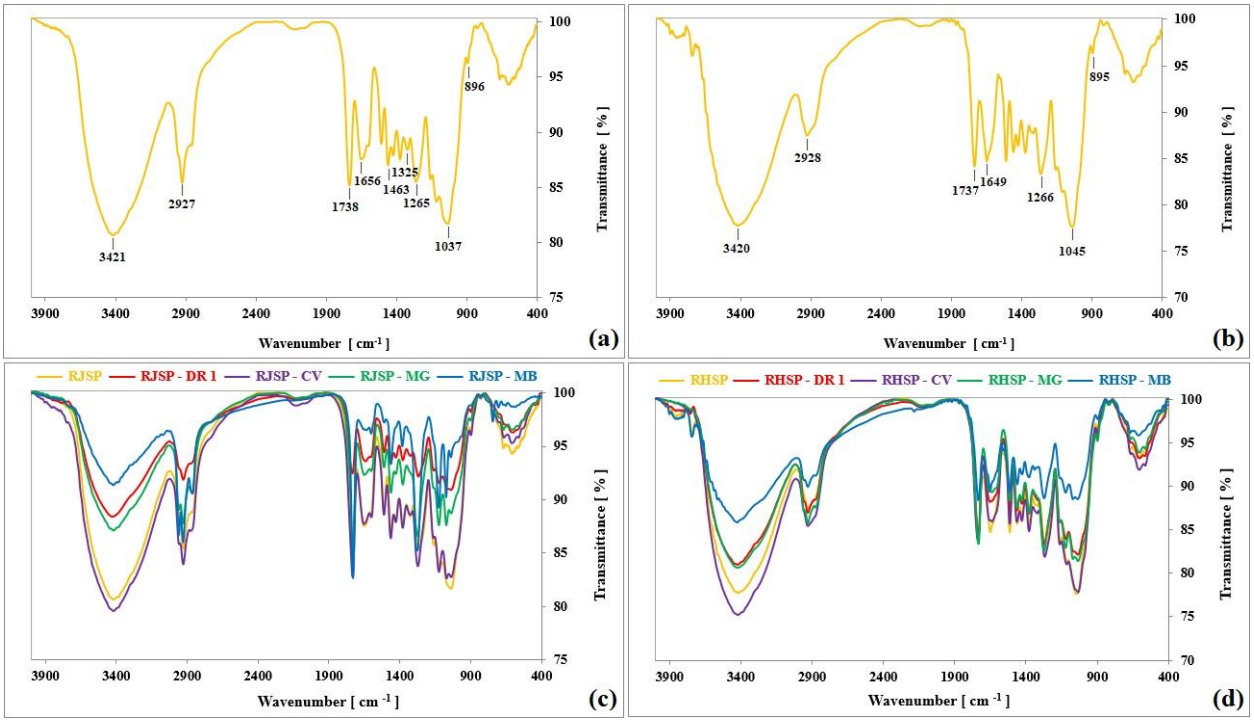


Fig.1 The FT-IR spectra of RJSP (a) RHSP (b), dyes-adsorbed RJSP (c), and dyes-adsorbed RHSP (d)

3.1.2. The BET analysis of green adsorbents

The BET graphs of RJSP and RHSP are shown in Fig.2 According to the BET analysis, RJSP has a specific surface area of 65.587 m^2/g, a total pore volume of 0.499 cm^3/g, and an average pore diameter of 0.701 nm, whereas the corresponding values for RHSP are 42.136 m^2/g, 0.504 cm^3/g, and 0.697 nm. The results indicate that RJSP and RHSP exhibit a mesoporous structure consistent with a type-IV isotherm, confirming their effective adsorbing a variety of environmental pollutants.

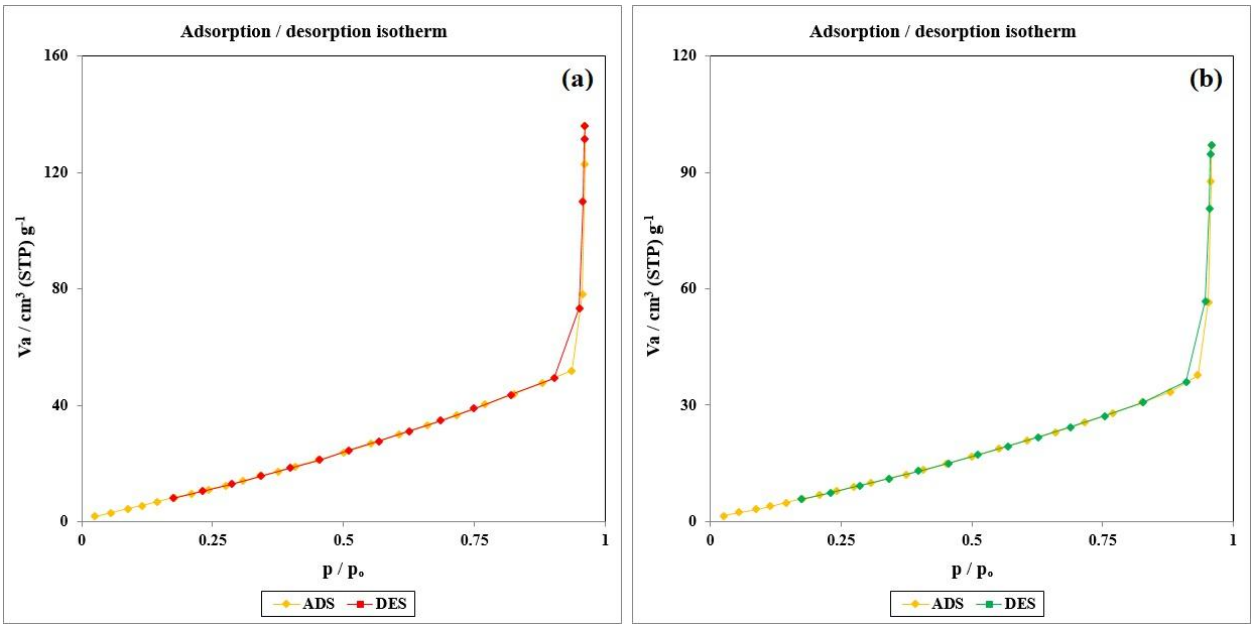


Fig.2 The nitrogen adsorption-desorption isotherm of RJSP (a) and RHSP (b)

3.1.3. The EDX analysis of green adsorbents

The EDX analyses of RJSP and RHSP are illustrated in Fig.3. Fig.3 (a) presents the EDX image of RJSP, confirming the presence of C (58.97%), N (4.31%), O (34.73%), Na (0.66%), Cl (0.71%), and Ca (0.62%). According to Fig.3 (b), RHSP mainly contains C (62.13%), O (33.43%), K (2.15%) and Ca (2.29%).

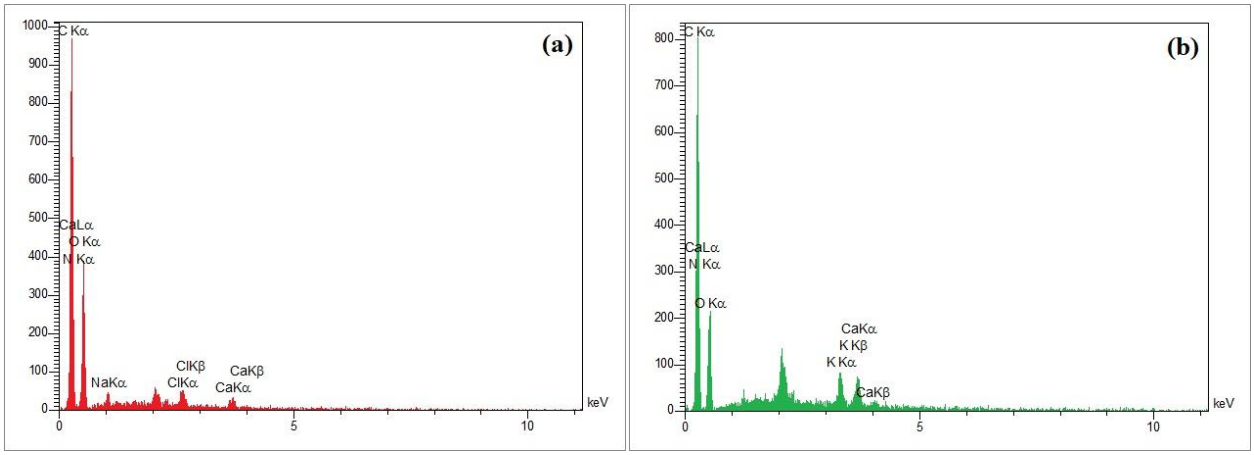


Fig.3 The EDX analysis of RJSP (a) and RHSP (b)

3.1.4. The morphological of green adsorbents

The morphology of RJSP and RHSP was investigated using FESEM. The FESEM images of RJSP, DR1-adsorbed-RJSP, RHSP, and MB-adsorbed-RHSP at two different magnifications are presented in Fig.4. As illustrated in Fig.4 (a), the RJSP shows cavity-like, layered, and cloud-like structural features. In addition, the FESEM images of DR1-adsorbed RJSP (Fig.4 (b)) show that dye adsorption changed the surface morphology of RJSP, and the cavity, layered, and cloud-like structures became smoother. As shown in Fig.4 (c), the RHSP had cavity-like, layered, and string-like structures. The FESEM images of MB-adsorbed RHSP (Fig.4 (d)) indicate that dye adsorption changed the surface morphology of RHSP, making the cavity-like, layered, and string-like structures smoother due to dye coverage. Also, the TEM images of RJSP and RHSP are shown in Fig.5. Fig.5 (a) shows the nanostructure of RJSP with cavity and cloud morphology. Fig.5 (b) further reveals the nanostructure of RHSP, exhibiting a layered morphology with cavity-like features.

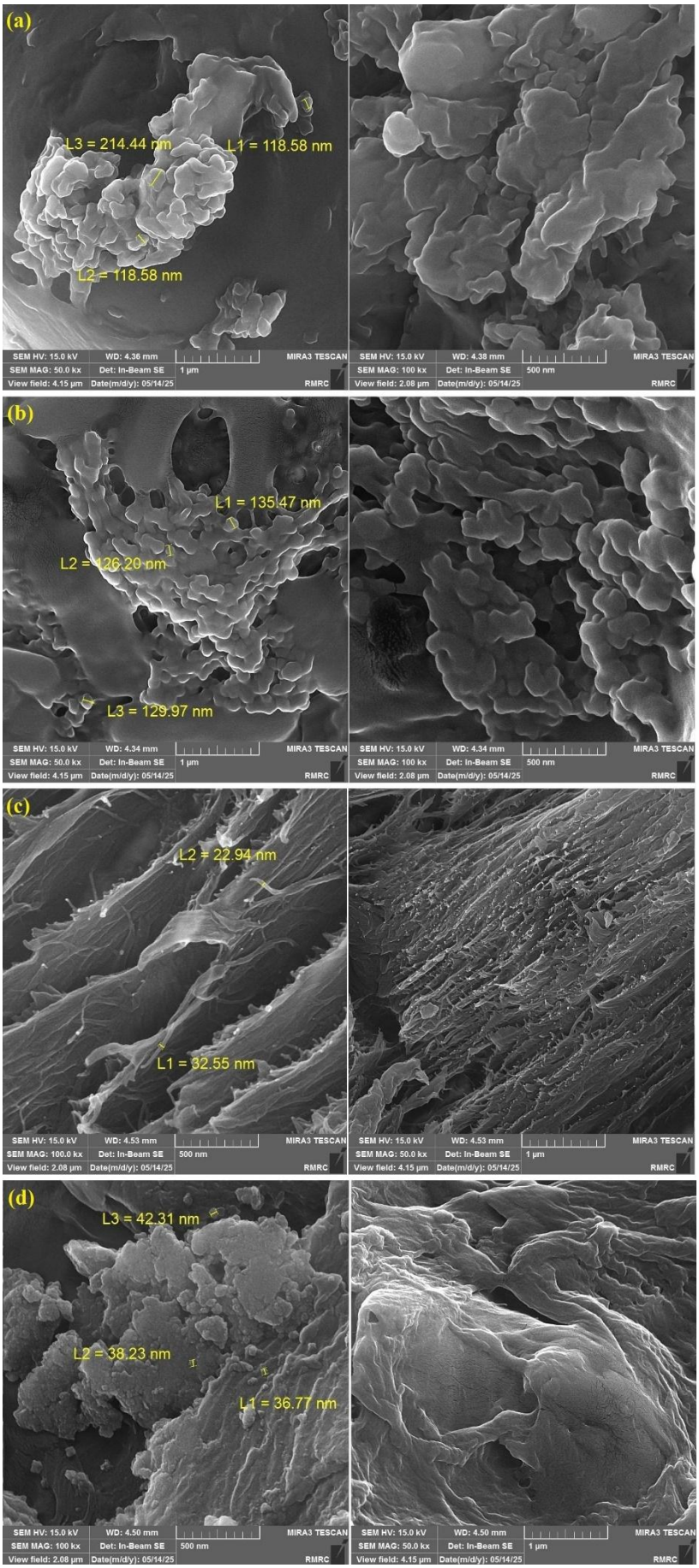

(a)
L3 = 214.44 nm
L1 = 118.58 nm
L2 = 118.58 nm
SEM HV: 15.0 kV
WD: 4.36 mm
MIRA3 TESCAN
SEM MAG: 50.0 kx
Det: In-Beam SE
1 µm
View field: 4.15 µm
Date(m/d/y): 05/14/25
RMRC
SEM HV: 15.0 kV
WD: 4.38 mm
MIRA3 TESCAN
SEM MAG: 100 kx
Det: In-Beam SE
500 nm
View field: 2.08 µm
Date(m/d/y): 05/14/25
RMRC
(b)
L1 = 135.47 nm
L2 = 126.20 nm
L3 = 129.97 nm
SEM HV: 15.0 kV
WD: 4.34 mm
MIRA3 TESCAN
SEM MAG: 50.0 kx
Det: In-Beam SE
1 µm
View field: 4.15 µm
Date(m/d/y): 05/14/25
RMRC
SEM HV: 15.0 kV
WD: 4.34 mm
MIRA3 TESCAN
SEM MAG: 100 kx
Det: In-Beam SE
500 nm
View field: 2.08 µm
Date(m/d/y): 05/14/25
RMRC
(c)
L2 = 22.94 nm
L1 = 32.55 nm
SEM HV: 15.0 kV
WD: 4.53 mm
MIRA3 TESCAN
SEM MAG: 100.0 kx
Det: In-Beam SE
500 nm
View field: 2.08 µm
Date(m/d/y): 05/14/25
RMRC
SEM HV: 15.0 kV
WD: 4.53 mm
MIRA3 TESCAN
SEM MAG: 50.0 kx
Det: In-Beam SE
1 µm
View field: 4.15 µm
Date(m/d/y): 05/14/25
RMRC
(d)
L3 = 42.31 nm
L2 = 38.23 nm
L1 = 36.77 nm
SEM HV: 15.0 kV
WD: 4.50 mm
MIRA3 TESCAN
SEM MAG: 100 kx
Det: In-Beam SE
500 nm
View field: 2.08 µm
Date(m/d/y): 05/14/25
RMRC
SEM HV: 15.0 kV
WD: 4.50 mm
MIRA3 TESCAN
SEM MAG: 50.0 kx
Det: In-Beam SE
1 µm
View field: 4.15 µm
Date(m/d/y): 05/14/25
RMRC

Fig.4 The FESEM images of RJSP (a) DR1-adsorbed RJSP (b), RHSP (c), and MB-adsorbed-RHSP (d)

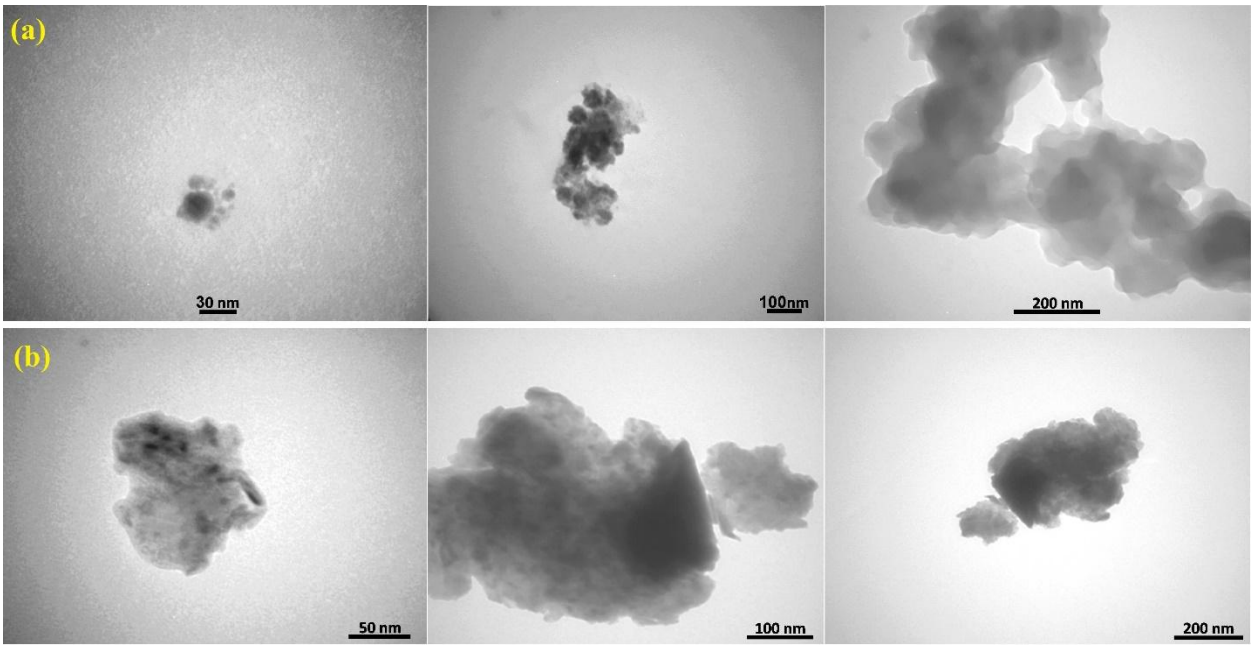


Fig.5 The TEM images of RJSP (a) and RHSP (b)

3.1.5. The determination of zero charge point pH (pH_{PZC})

The surface characteristics of the prepared materials were further evaluated by measurement of the point of zero charge (pH_{PZC}) [18]. The pH_{PZC} of RJSP and RHSP was determined over the pH range of 3.0-12.0. As illustrated in Fig.6, the pH_{PZC} values of RJSP and RHSP are found to be pH 7.37 and 7.35, respectively. The surface charge of both RJSP and RHSP is pH-dependent, with positive surface charges below the pH_{PZC} and negative surface charges above it.

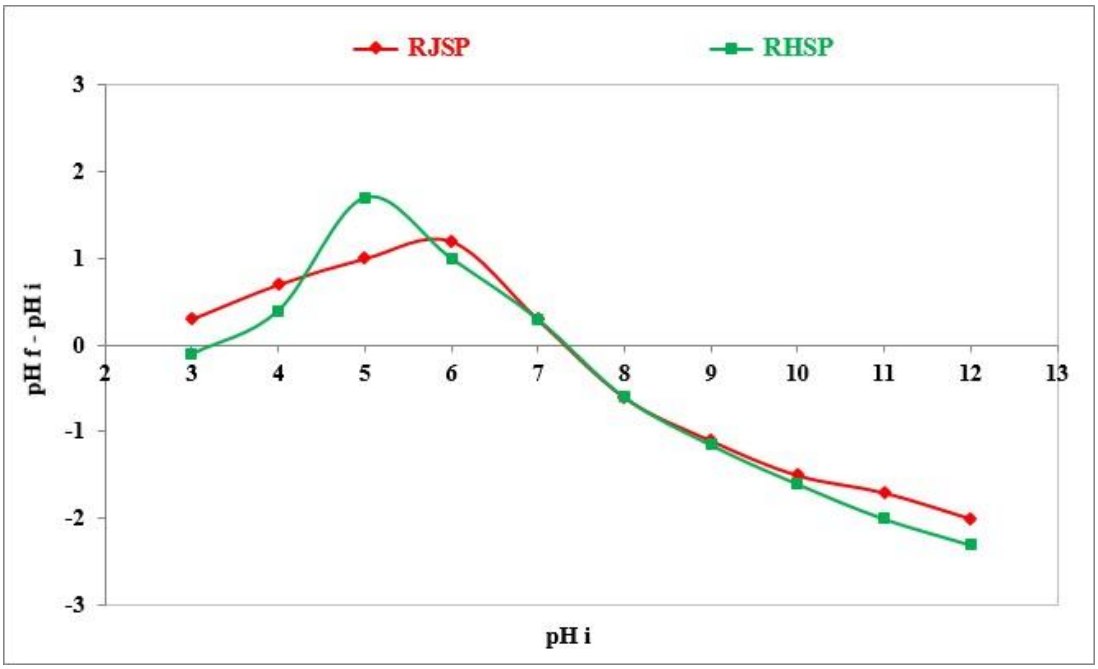


Fig.6 The determination of pH_{pzc} for the RJSP and RHSP

3.2. Optimization of the dye adsorption performance of green adsorbents

3.2.1. The effect of pH

The adsorption performances of RJSP and RHSP were evaluated over the pH range 3.0–12.0. As presented in Fig.7 (a, b), the adsorption capacities of RJSP and RHSP increases as pH rises from 3.0 to 9.0. The optimal pH range for maximum dye adsorption by RJSP and RHSP was found to be 7.0 to 9.0. In acidic solutions ($pH < pH_{PZC}$), the RJSP and RHSP exhibit low adsorption capacity due to repulsive interactions with cationic dye molecules. Moreover, at acidic pH, the high concentration of H^+ ions limit the adsorption of cationic dye molecules by competing for the available adsorption sites, leading to lower removal efficiency [18,37]. The enhanced adsorption of cationic dyes by RJSP and RHSP at pH values above the pH_{PZC} results from stronger electrostatic attraction forces. Such electrostatic interactions are due to the negatively charged active sites present on the surfaces of RJSP and RHSP [38,39]. The enhanced

adsorption efficiency of MB, MG, CV, and DR1 dyes can be attributed to ionic interactions with the anionic surfaces of RJSP and RHSP. Consequently, pH values of 9.0, 8.0, 7.0, and 8.0 were selected as the optimal conditions for MB, MG, CV, and DR1 adsorption, respectively, on both RJSP and RHSP.

3.2.2. The effect of time

Fig.7 (c, d) illustrates how contact time affects the adsorption performance of dyes onto RJSP and RHSP. The adsorption capacity of the RJSP and RHSP gradually increased with contact time due to the abundance of active sites at the beginning of the adsorption process. As time progresses, dye molecules diffuse into internal adsorption sites, and the adsorption process gradually reaches equilibrium [17,18]. Based on the results, the optimum contact times for the adsorption of MB, MG, CV, and DR1 onto RJSP were determined to be 16, 14, 14, and 14 min, respectively, whereas the corresponding values for RHSP were 14, 12, 12, and 14 min.

3.2.3. The effect of bio-adsorbent dosage

To evaluate adsorption efficiency, the influence of RJSP and RHSP dosage on dye removal was investigated. As illustrated in Fig.7 (e, f), raising the adsorbent dosage from 0.003 to 0.021 g enhances dye adsorption by both RJSP and RHSP. This behavior can be attributed to the presence of unoccupied cavities and additional active sites on the RJSP and RHSP. It was observed that further increments in the RJSP and RHSP did not lead to any noticeable improvement in dye adsorption. A possible explanation for this behavior is the aggregation or overlap of RJSP and RHSP particles, which reduces the surface area available for adsorption [17,18]. Based on the obtained results, the optimum dosages of RJSP for MB, MG, CV, and DR1

adsorption were 0.020, 0.015, 0.018, and 0.018 g respectively, while the corresponding dosages for RHSP were 0.020, 0.018, 0.018, and 0.018 g.

3.2.4. The effect of temperature

To evaluate the role of temperature, adsorption experiments were investigated over the temperature range of 25–85 °C. As Fig.7 (g) shows, the adsorption capacities of all four dyes gradually decreased with increasing temperature from 25 °C to 85 °C. Based on the experimental results, the adsorption of all four dyes was most efficient at 25 °C. Thus, the adsorption process in this system is exothermic. As presented in Fig.7 (h), the adsorption performance of all four dyes improved with increasing temperature over the range of 25-85 °C. Based on the experimental results, the adsorption of all four dyes was most efficient at 65 °C. Thus, the adsorption process in this system is endothermic. Furthermore, the increased adsorption rate at higher temperatures can be attributed to improved dye diffusion and decreased viscosity of the solution in the presence of RHSP. Additionally, the adsorption capacity increased with temperature, which may be associated with faster molecular diffusion of the dyes. The experimental results reveal that dye adsorption follows an endothermic process [17,18].

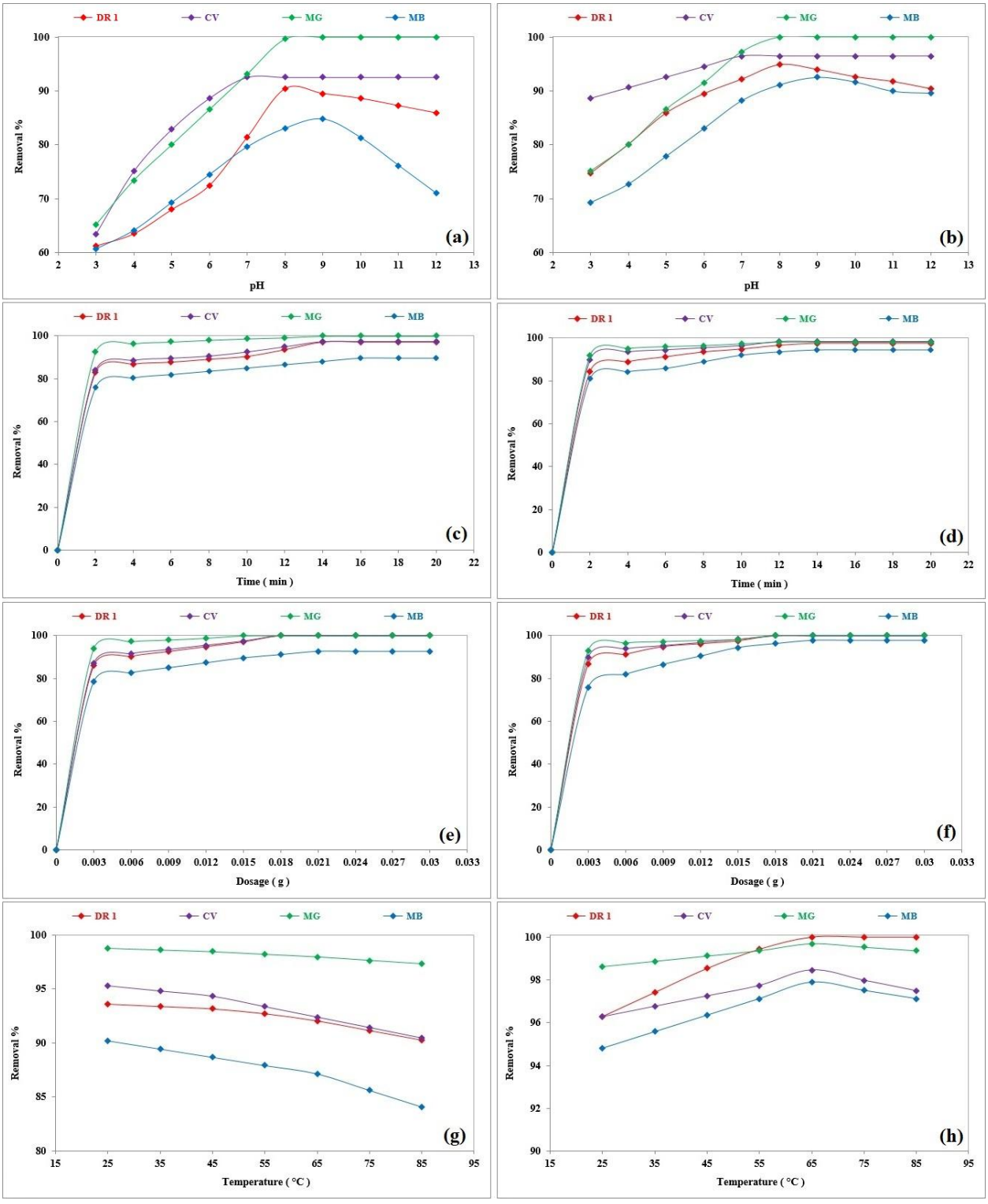

DR 1
CV
MG
MB
Removal %
pH
(a)
(b)
Time (min)
(c)
(d)
Dosage (g)
(e)
(f)
Temperature (°C)
(g)
(h)

Fig.7 The effect of pH for the RJSP (a) and RHSP (b); time for the RJSP (c) and RHSP (d); bio-adsorbent dosage for the RJSP (e) and RHSP (f); and temperature for the RJSP (g) and RHSP (h) on the adsorption of dyes

3.2.5. The effect of initial dye concentration

To evaluate the influence of the initial dye concentration, MB, MG, CV, and DR1 solutions with concentrations ranging from 50 to 200 mg/L were prepared. Fig.8 illustrates that increasing the initial dye concentration enhanced the adsorption capacities of both RJSP and RHSP. An inverse relationship is observed between initial dye concentration and removal efficiency. At relatively low initial dye concentrations, a greater number of dye molecules can occupy the active sites on RJSP and RHSP adsorbents, leading to enhanced adsorption. This behavior is likely related to the greater number of unoccupied adsorption sites at lower initial dye concentrations [17,18].

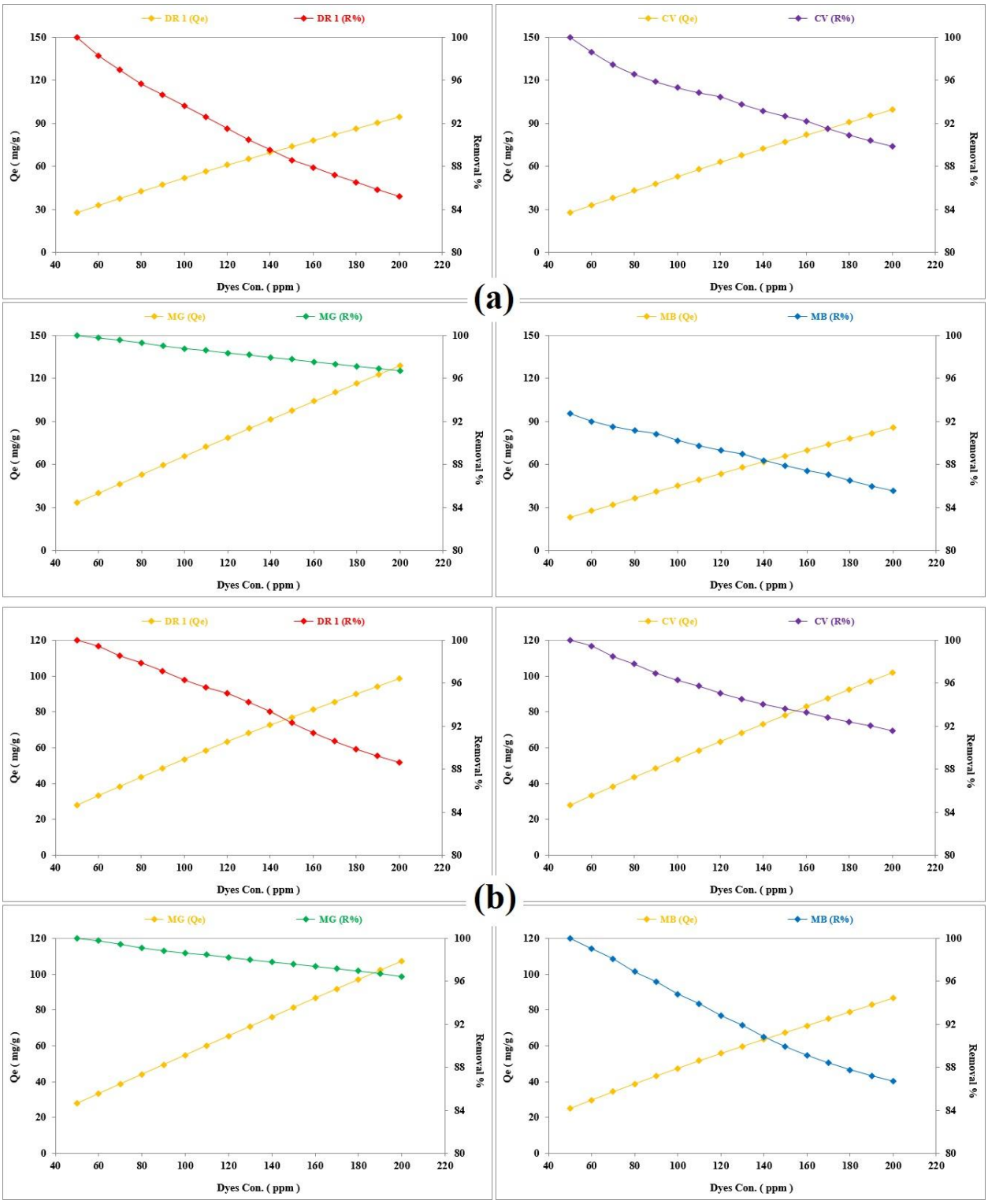


Fig.8 The effect of initial dye concentration on the dye removal by RJSP (a) and RHSP (b) (The optimal conditions: pH, time, bioadsorbent dosage, and temperature)

3.3. The adsorption kinetics

The adsorption kinetics were studied to better understand both the adsorption rate and its mechanism. The pseudo-first-order, pseudo-second-order, Weber-Morris, and Elovich models were applied to investigate the adsorption mechanism and identify the rate-limiting step of dye adsorption on RJSP and RHSP [40–42].

The adsorption data shown in Fig.7 (c, d) were used to derive linear relationships for pseudo-first-order (Fig. S1, Supplementary information) and pseudo-second-order (Fig. S2, Supplementary information) models. Table 1 summarizes the kinetic parameters obtained from the four kinetic models. Among the evaluated kinetic models, the adsorption behavior of all dyes was better described by the pseudo-second-order kinetic model. Furthermore, the q_e values predicted by the pseudo-second-order model closely corresponded to the experimental q_e values [43].

Fig. S3 (Supplementary information) demonstrates the plot of q_t as a function of $t^{0.5}$. As shown in Fig.7 (c, d), intraparticle diffusion occurs in three stages. However, because the first stage occurs rapidly, it was excluded from the calculations, and only the gradual stage was considered. This behavior suggests the presence of two distinct stages in the adsorption process of dyes by the RJSP and RHSP systems. The dual linearity highlights the effect of two different stages in the adsorption mechanism, likely reflecting different stages of dye interaction with the material surfaces. This result indicates that intraparticle diffusion plays a significant role in the adsorption of dyes onto RJSP and RHSP [44].

The Elovich model is commonly used to evaluate chemisorption kinetics on energetically heterogeneous solid surfaces. According to Table 1 and Fig. S4 (Supplementary information), R^2

values for MB and MG indicate that their adsorption onto RJSP is well described by the Elovich model. In contrast, the relatively low R^2 values obtained for the adsorption of CV and DR1 onto RJSP indicate a poor fit of the Elovich model. The R^2 values show that the adsorption of MG, CV, and DR1 onto RHSP is well described by the Elovich model, whereas the low R^2 value for MB suggests that this model does not adequately describe its adsorption behavior. Overall, based on the Elovich model, the surfaces of RJSP and RHSP are considered to be heterogeneous.

Table 1. The kinetic parameters for the adsorption of dyes on RJSP and RHSP

RJSP	**Pseudo-first-order kinetic model**				**Pseudo-second-order kinetic model**			
	Q_e (mg/g)	K_1 (1/min)	Q_{cal} (mg/g)	R^2	Q_e (mg/g)	K_2 (g/(mg.min))	Q_{cal} (mg/g)	R^2
DR1	32.360	0.1019	5.242	0.8343	32.360	0.0899	31.513	0.9983
CV	32.470	0.1329	5.259	0.8761	32.470	0.0888	32.115	0.9988
MG	33.350	0.1715	2.380	0.9827	33.350	0.2138	33.373	0.9999
MB	29.880	0.1528	5.856	0.9267	29.880	0.0715	29.973	0.9990
RHSP	**Pseudo-first-order kinetic model**				**Pseudo-second-order kinetic model**			
	Q_e (mg/g)	K_1 (1/min)	Q_{cal} (mg/g)	R^2	Q_e (mg/g)	K_2 (g/(mg.min))	Q_{cal} (mg/g)	R^2
DR1	32.500	0.2572	8.959	0.9454	32.500	0.0608	33.275	0.9994
CV	32.800	0.1345	2.722	0.9748	32.800	0.2087	32.488	0.9999
MG	32.700	0.1753	1.918	0.9439	32.700	0.2986	32.648	0.9999
MB	31.470	0.2473	9.116	0.8857	31.470	0.0573	32.183	0.9981

RJSP	**Elovich kinetic model**			**Weber-Morris kinetic model**		
	β (g/mg)	α (mg/(g.min))	R^2	C (mg/g)	K_d (mg/(g.min$^{0.5}$))	R^2
DR1	0.810	$5.417\times10^{+9}$	0.7866	26.7289	1.1344	0.8740
CV	0.726	$7.513\times10^{+8}$	0.8799	27.0089	1.2409	0.9400

MG	1.407	$8.694 \times 10^{+18}$	0.9744	30.9096	0.6270	0.9983
MB	0.645	$1.424 \times 10^{+7}$	0.9269	24.2357	1.3232	0.9827
RHSP	**Elovich kinetic model**			**Weber-Morris kinetic model**		
	β (g/mg)	α (mg/(g.min))	R^2	C (mg/g)	K_d (mg/(g.min$^{0.5}$))	R^2
DR1	0.433	$2.066 \times 10^{+5}$	0.9756	25.2759	2.0248	0.9888
CV	1.276	$4.295 \times 10^{+16}$	0.9473	29.7470	0.7387	0.9871
MG	1.794	$8.261 \times 10^{+23}$	0.9443	30.7025	0.5253	0.9832
MB	0.494	$6.449 \times 10^{+5}$	0.8772	24.6054	1.8333	0.9465

3.4. The adsorption isotherms

In this study, the adsorption performance of MB, MG, CV, and DR1 dyes on RJSP and RHSP was analyzed using the Temkin, Freundlich, and Langmuir models [45–48]. Table 2 provides the adsorption isotherm parameters, and the fitting curves for the three isotherm models are presented in Fig. S5–S7 (Supplementary information). The obtained data indicate that the adsorption of four dyes is most accurately described by the Freundlich isotherm. It is evident that the heterogeneous surfaces possess different functional groups, which leads to adsorption with different energies. The data reported in Table 2 reveal that the 1/n values for four dyes are below one, suggesting that the adsorption onto RJSP and RHSP is favorable. The R_L values were all below 1.0, indicating favorable adsorption of the four dyes [46]. Moreover, the n values are greater than one, indicating that the adsorption occurs through favorable physical interactions [47]. The calculated Q_m values for MB, MG, CV, and DR1 were 145, 124, 114, and 98 mg/g on RJSP, whereas the corresponding values for RHSP were 84, 111, 102, and 94 mg/g, respectively. Furthermore, the obtained parameters from the Temkin isotherm indicate relatively high binding

constants for both RJSP and RHSP [48]. Table 3 compares the optimum pH, the maximum adsorption capacity, and the equilibrium time of RJSP and RHSP with those reported for other adsorbents.

Table 2. The Langmuir, Freundlich and Temkin isotherm model parameters

RJSP	**Langmuir constants**			
	Q_m (mg/g)	K_L (L/mg)	R_L	R^2
DR1	98	0.199	0.091	0.9439
CV	114	0.201	0.091	0.9733
MG	124	1.162	0.017	0.9083
MB	145	0.047	0.298	0.9978
RHSP	**Langmuir constants**			
	Q_m (mg/g)	K_L (L/mg)	R_L	R^2
DR1	94	0.449	0.043	0.9195
CV	102	0.361	0.052	0.9093
MG	111	0.822	0.024	0.9458
MB	84	0.302	0.062	0.9174
RJSP	**Freundlich constants**			
	n	1/n	K_F ((mg/g) (L/mg)$^{1/n}$)	R^2
DR1	2.6868	0.3722	26.111	0.9959
CV	2.3365	0.4280	27.616	0.9993
MG	2.2109	0.4523	56.378	0.9908
MB	1.6629	0.6014	11.460	0.9987
RHSP	**Freundlich constants**			
	n	1/n	K_F ((mg/g) (L/mg)$^{1/n}$)	R^2
DR1	3.1824	0.3142	36.082	0.9976

CV	2.5511	0.3920	32.621	0.9897
MG	2.2943	0.4359	46.352	0.9935
MB	2.9634	0.3375	27.514	0.9924
RJSP	**Temkin constants**			
	b_T (J/mol)	B_T	K_T (L/mg)	R^2
DR1	102.229	24.2356	1.370	0.9699
CV	85.256	29.0602	1.370	0.9874
MG	66.471	37.2729	4.394	0.9897
MB	70.831	34.9785	0.375	0.9927
RHSP	**Temkin constants**			
	b_T (J/mol)	B_T	K_T (L/mg)	R^2
DR1	116.927	21.1891	3.651	0.9769
CV	92.732	26.7175	2.142	0.9547
MG	79.755	31.0649	4.048	0.9916
MB	123.786	20.0149	2.182	0.9611

Table 3. The comparison of RJSP and RHSP with other adsorbents for the adsorption of dyes

Dye	Adsorbent	Q_m (mg/g)	Time (min)	pH	Reference
DR1	RJSP	98	14	8	This work
	RHSP	94	14	8	This work
	RSSSP	85	14	7	3
	TiO_2/Gly/*β*-CD NPs	139	15	9	17
	TiO_2/γCD NPs	238	10	9	18
	MWCNTs/Gly/β-CD	500	5	7	49
CV	RJSP	114	14	7	This work
	RHSP	102	12	7	This work
	RSSSP	81	14	7	3
	TiO_2/γCD NPs	213	10	9	18
	BOH/Gly/βCD NPs	97.40	21	8	4
	BOH/NH_2/βCD NPs	104.14	18	8	4

	ESh/Gly/βCD NPs	94.58	21	8	16
	ESh/NH_2/βCD NPs	101.19	18	8	16
	Nascent Rice Husk (RH)	25.46	1440	7	50
	GG/$NiWO_4$	170.42	50	7	51
	TSCB composite	107.53	30	7	52
	Apple stem	154	20	10	53
MG	RJSP	124	14	8	This work
	RHSP	111	12	8	This work
	RSSSP	120	12	8	3
	TiO_2/γCD NPs	244	10	7	18
	BOH/Gly/βCD NPs	102.93	21	8	4
	BOH/NH_2/βCD NPs	102.32	18	8	4
	ESh/Gly/βCD NPs	103.09	21	8	16
	ESh/NH_2/βCD NPs	101.55	18	8	16
	GALA	113.50	720	8	54
	Chitosan-DES B	17.86	20	9	55
	Nymphaea lotus (WLSAB)	102.35	30	7	56
	Tapioca peel (S@TP)	30.18	120	8	57
MB	RJSP	145	16	9	This work
	RHSP	84	14	9	This work
	RSSSP	98	14	8	3
	TiO_2/γCD NPs	134	20	9	3
	TiO_2/Gly/*β*-CD NPs	82	30	8	13
	MWCNTs/Gly/β-CD	90.90	20	8	49
	Nascent Rice Husk (RH)	24.48	180	7	50
	TSCB composite	112.87	30	8	52
	Walnut shell powder	36.63	200	8	58
	Argania shells	90.96	240	8	59

3.5. The thermodynamic study

The thermodynamic behavior of MB, MG, CV, and DR1 adsorption on RJSP and RHSP was evaluated at temperatures ranging from 298 to 328 K [18]. The thermodynamic parameters obtained for adsorption on RJSP and RHSP are presented in Table 4, while the related plots are provided in Fig. S8 (Supplementary information). The thermodynamic data presented Table 4 indicate that the adsorption of the studied dyes onto RJSP and RHSP is thermodynamically spontaneous, as evidenced by the negative ΔG° values. The absolute values of ΔG° increased

with temperature, indicating that the adsorption process became more thermodynamically favorable. Furthermore, the observed ΔGº range (-20–0 kJ/mol) confirms that the adsorption of MB, MG, CV, and DR1 proceeds through a spontaneous physisorption process [60].

Negative ΔH° values for all dyes confirm that the adsorption on RJSP is exothermic, which explains the inverse relationship between adsorption and temperature [61]. In contrast, the positive ΔH° values obtained for all dyes indicate that the adsorption on RHSP is endothermic, supporting the observed enhancement in adsorption capacity at higher temperatures [18].

Furthermore, the negative ΔS° values indicate a decrease in molecular disorder at the solid–solution interface during the adsorption of all dyes onto RJSP. Meanwhile, the positive ΔS° values indicate that the solid–solution interface becomes more disordered during the adsorption of all dyes onto RHSP. However, the number of water molecules desorbed from RHSP exceeded the number of dye molecules adsorbed, resulting in an overall increase in entropy [18].

Table 4. The thermodynamic parameters for the adsorption of dyes on the RJSP and RHSP

RJSP			ΔG° (kJ/mol)			
Dye	ΔH° (kJ/mol)	ΔS° (J/mol.K)	T = 298 K	T = 308 K	T = 318 K	T = 328 K
DR1	-6.797	-4.902	-5.198	-5.278	-5.354	-5.337
CV	-11.638	-18.546	-6.003	-5.939	-5.882	-5.607
MG	-12.110	-7.124	-9.908	-9.910	-9.928	-9.828
MB	-7.947	-13.725	-3.789	-3.701	-3.613	-3.524
RHSP			ΔG° (kJ/mol)			
Dye	ΔH° (kJ/mol)	ΔS° (J/mol.K)	T = 298 K	T = 308 K	T = 318 K	T = 328 K
DR1	50.918	191.817	-6.620	-7.794	-9.580	-12.492

CV	13.786	68.269	-6.602	-7.194	-7.871	-8.661
MG	21.023	100.891	-9.137	-9.957	-10.941	-12.190
MB	16.463	73.459	-5.487	-6.102	-6.826	-7.706

3.6. The desorption and reuse

The regeneration behavior of RJSP and RHSP was evaluated by performing desorption experiments in a batch system. To regenerate RJSP and RHSP during the desorption processes, various eluting agents, including 0.1 M HCl, 0.1 M NaOH, acetonitrile, ethanol, and methanol, were used (Fig.9 (a, b)). Among the tested eluting agents, ethanol and methanol provided the highest regeneration efficiencies for both RJSP and RHSP, especially ethanol. Thus, ethanol was selected as the elution agent for further tests.

Fig.9 (c, d) illustrates the adsorption performance of RJSP and RHSP over five adsorption-desorption cycles. The adsorption capacities of RJSP and RHSP for all dyes gradually decreased with each reuse. Following five adsorption-desorption cycles, the removal efficiencies of MB, MG, CV, and DR1 were 81, 90, 93, and 86 % onto RJSP, while the corresponding values for RHSP were 87, 92, 93, and 91 %, respectively.

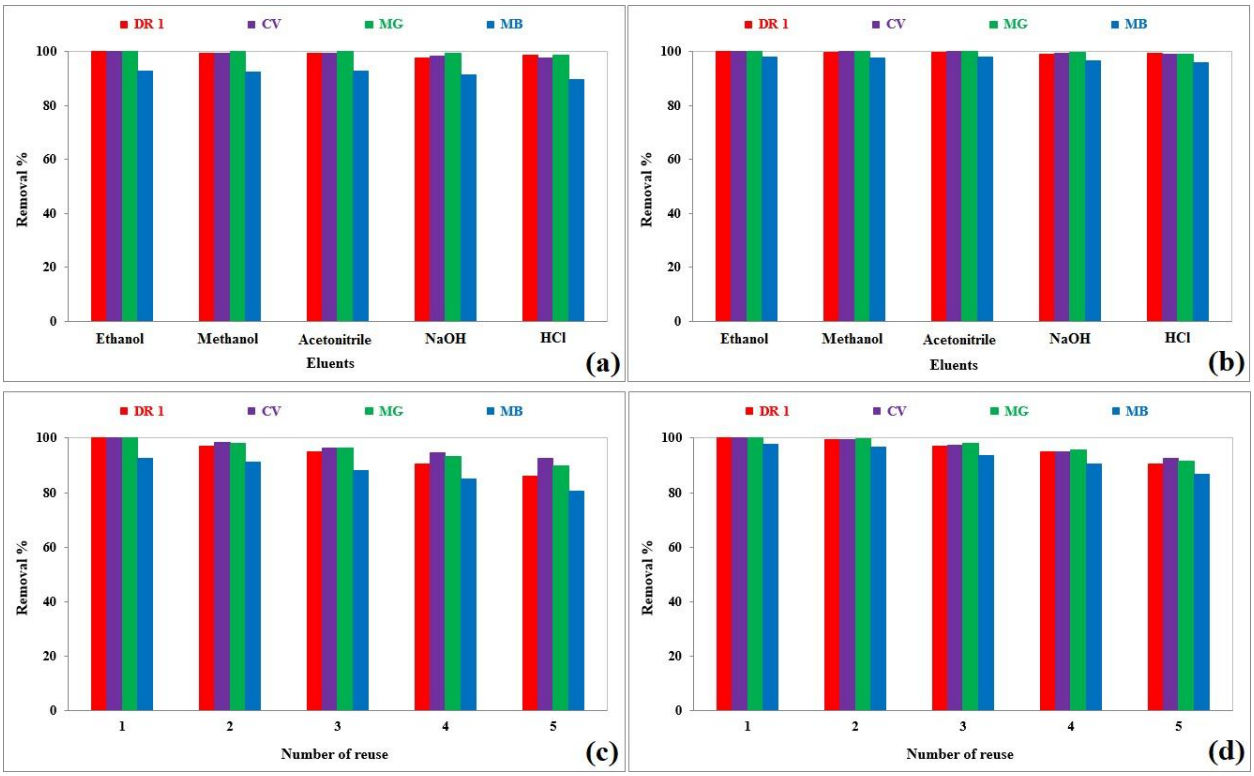


Fig.9 The desorption efficiency plots of dyes using various eluents onto RJSP (a) and RHSP (b); and cycle adsorption–desorption experiments of dyes by RJSP (c) and RHSP (d) in ethanol (The optimal conditions: pH, time, bioadsorbent dosage, and temperature, and initial dye concentration: 50 mg/L)

3.7. The adsorption mechanism

The adsorption mechanism depends on several factors, including the surface chemistry of RJSP and RHSP, the nature of interactions with the dyes, solution pH, and the results from isotherm, kinetic, and thermodynamic analyses. The effect of pH provides valuable information on the adsorption behavior. Increased dye adsorption by RJSP and RHSP at pH values above the pH_{PZC} ($pH > pH_{PZC}$) likely results from enhanced electrostatic attraction of the dye molecules to the adsorbent surfaces. This electrostatic attraction arises from the negatively charged surface

sites of RJSP and RHSP. Moreover, the interaction of dyes with the anionic surfaces RJSP and RHSP through ionic complex formation is expected to enhance adsorption efficiency.

During the adsorption process, adsorbate molecules are initially transported to the adsorbent's outer surface and subsequently diffuse through the boundary layer before entering the internal adsorption sites. The Freundlich isotherm model describes the surface of the adsorbent is heterogeneous and contains different functional groups that provide sites with different adsorption energies. The thermodynamic results revealed negative $\Delta G°$ values (-20 to 0 kJ/mol), revealing that the adsorption of the studied dyes onto RJSP and RHSP occurs spontaneously through a physical adsorption. Negative $\Delta H°$ values obtained for all dyes demonstrate exothermic nature of adsorption on RJSP, which explains the inverse relationship between adsorption capacity and temperature. Meanwhile, positive $\Delta H°$ values for all dyes confirm that adsorption on RHSP is endothermic, in agreement with the enhanced adsorption capacity observed at higher temperatures. Furthermore, the negative $\Delta S°$ values indicate a reduction in disorder at the solid/solution interface throughout the adsorption of all dyes onto RJSP. In contrast, the positive $\Delta S°$ values indicate that dye adsorption onto RHSP leads to greater disorder at the solid–solution interface. However, the number of water molecules desorbed from RHSP exceeded the number of dye molecules adsorbed, resulting in an overall increase in entropy. Fig.10 presents the adsorption mechanism for dyes on the green adsorbents (RJSP and RHSP).

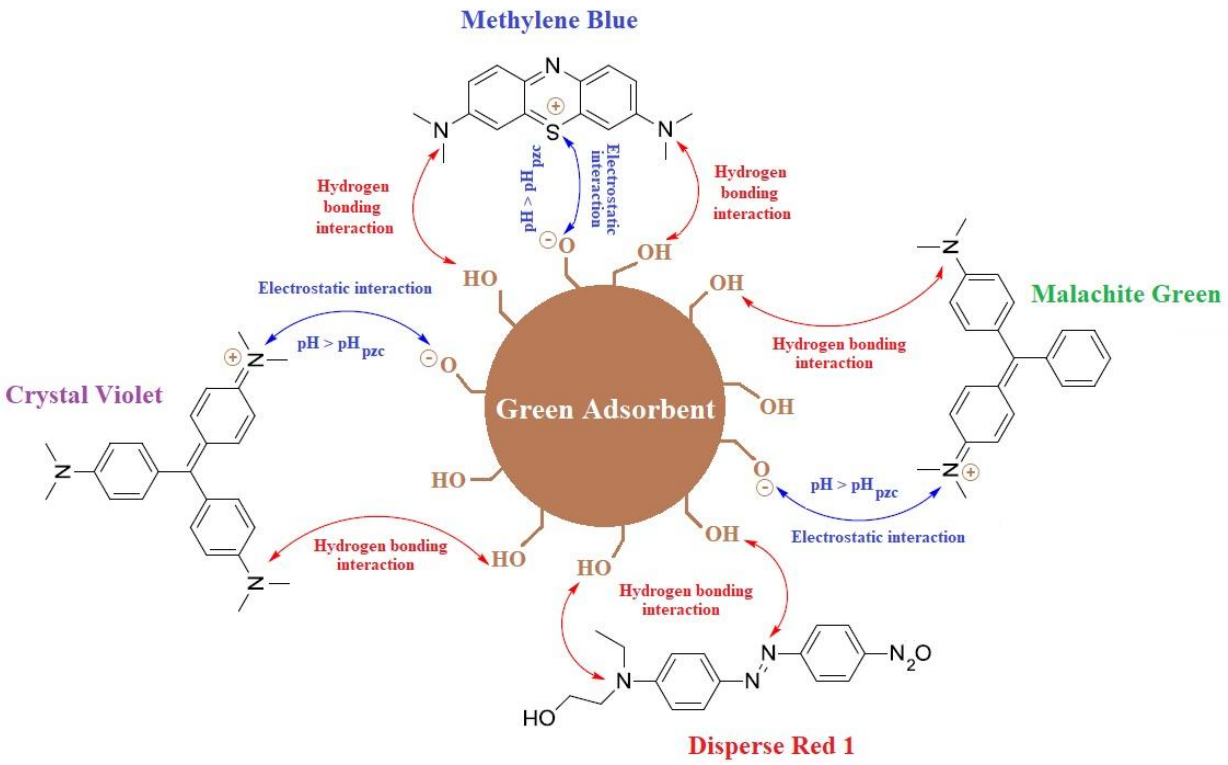


Fig.10 The adsorption mechanism for dyes on the green adsorbents (RJSP and RHSP)

4. Conclusion

In this study, the raw jujube stone particles (RJSP) and the raw hawthorn stone particles (RHSP) were investigated as efficient, natural, and environmentally friendly adsorbents for the removal of MB, MG, CV, and DR1 dyes. The BET-specific surface area, total pore volume, and average pore diameter of RJSP were 65.587 m^2/g, and 0.499 cm^3/g, 0.701 nm, respectively, whereas the corresponding values for RHSP were 42.136 m^2/g, and 0.504 cm^3/g, 0.697 nm. After completing five consecutive adsorption-desorption cycles, the removal efficiencies of MB, MG, CV, and DR1 were 81, 90, 93, and 86 % for RJSP, and 87, 92, 93 and 91 % for RHSP, respectively. The adsorption behavior of MB, MG, CV, and DR1 on RJSP and RHSP was found to follow the Freundlich isotherm and pseudo-second-order kinetic models. Also, according to

the Langmuir isotherm, the Q_m values for MB, MG, CV, and DR1 were 145, 124, 114, and 98 mg/g on RJSP, while the corresponding values on RHSP were 84, 111, 102, and 94 mg/g, respectively. In addition, the thermodynamic results indicated that the adsorption of MB, MG, CV, and DR1 onto RJSP is exothermic, whereas adsorption onto RHSP is endothermic. The thermodynamic and isotherm data demonstrate that the adsorption of MB, MG, CV, and DR1 dyes on RJSP and RHSP occurs via physical adsorption. Finally, the RJSP and RHSP could serve as efficient, cost-effective, natural, and environmentally friendly adsorbents for removing industrial dyes from wastewater.

Declarations

Ethical Approval

We declare that accepted principles of ethical and professional conduct have been followed.

Funding

This research did not receive any specific grant from funding agencies in the public, commercial, or not-for-profit sectors.

Competing Interests

The authors have no relevant financial or non-financial interests to disclose.

Acknowledgements

We appreciate University of Guilan for support of this work.

Data Availability Statement

I confirm that the data are original and obtained in our lab. All data generated or analysed during this study are included in this published article [and its Supplementary information (SI) files]. The curves of adsorption kinetics, curves of adsorption isotherms, and curves of adsorption thermodynamic (Figure S1-S8) in the Supplementary information. References 18, 40-42, and 45-48 are cited in the Supplementary information.

Author Contributions

All authors contributed to the study conception and design. Conceptualization, Methodology, Software, Data collection and analysis, Investigation, Validation, Supervision, Project administration, Writing - original draft, Writing - review & editing was performed by **Seyed Hossein Mousavi**. Visualization, Funding acquisition, Resources, Data collection and analysis, Investigation, editing was performed by **Susan Jafari**. Visualization, Data collection and analysis, Investigation, Writing - review & editing was performed by **Sahar Hanifehpour**. Conceptualization, Methodology, Supervision, Project administration, editing was performed by **Hadi Fallah Moafi**. The first draft of the manuscript was written by **Seyed Hossein Mousavi** and all authors commented on previous versions of the manuscript. All authors read and approved the final manuscript.

References

[1] Morais NA, Fernandes L, Ariana-Machado J, Capelo JL, Lodeiro C, Oliveira E (2017) An unusual emissive and colorimetric copper (II) detection by a selective probe based on a pseudo-crown cysteine dye: Solution and gas phase studies. Inorg Chem Commun 86:299–303. https://doi.org/10.1016/j.inoche.2017.11.001.

[2] Mousavi SH, Mohammadi A, Zanjanchi MA, Moafi HF (2025) Paper-based colorimetric chemosensor for highly sensitive and selective detection of Cd^{2+} in water and food samples. Anal Methods 17:9365–9380. https://doi.org/10.1039/D5AY01326G.

[3] Mousavi SH, Samakchi S, Kianfar M, Zahmatkesh M, Zohourtalab A (2022) Raw sunflower seed shell particles as a green adsorbent for the adsorption of synthetic organic dyes from wastewater. Environ Prog Sustainable Energy 7:e14017. https://doi.org/10.1002/ep.14017.

[4] Shabanian F, Sohrabnezhad S (2025) Boehmite Modified with β-Cyclodextrin as an Eco-friendly Adsorbent for the Removal of Toxic Organic Compounds. Phys Chem Res 13:319–336. https://doi.org/10.22036/pcr.2025.488346.2591.

[5] Hayoun B, Escudero-Curiel S, Bourouina M, Bourouina-Bacha S, Sanromán MA, Pazos M (2022) Preparation and characterization of high performance hydrochar for efficient adsorption of drugs mixture. J Mol Struct 353:118797. https://doi.org/10.1016/j.molliq.2022.118797.

[6] Haji A, Naebe M (2020) Cleaner dyeing of textiles using plasma treatment and natural dyes: A review. J Cleaner Prod 265:121866. https://doi.org/10.1016/j.jclepro.2020.121866.

[7] Aksu Z (2005) Application of biosorption for the removal of organic pollutants: a review. Process Biochem 40:997−1026. https://doi.org/10.1016/j.procbio.2004.04.008.

[8] Khandegar V, Saroha AK (2013) Electrocoagulation for the treatment of textile industry effluent–a review. J Environ Manage 128:949−963. https://doi.org/10.1016/j.jenvman.2013.06.043.

[9] Kouzi Y, Elidrissi ZC, Essate A, Beqqour D, Achiou B, Younssi SA, Rabiller-Baudry M, Bouhria M, Ouammou M (2025) Tailored rGO-TiO_2-pPD low-cost ceramic membrane for dye wastewater filtration: A synergistic strategy of GO reduction, intercalation and crosslinking. Sep Purif Technol 378:134643. https://doi.org/10.1016/j.seppur.2025.134643.

[10] Tabish M, Tabinda AB, Mazhar Z, Yasar A, Ansar J, Wasif I (2024) Physical, chemical and biological treatment of textile wastewater for removal of dyes and heavy metals. Desalin Water Treat 320:100842. https://doi.org/10.1016/j.dwt.2024.100842.

[11] Sotelo S, Oyarce E, Roa K, Boulett A, Pizarro G, Sánchez J (2024) Sodium lignosulfonate as an extracting agent of methylene blue dye using a polymer-enhanced ultrafiltration technique. Int J Biol Macromol 275:133567. https://doi.org/10.1016/j.ijbiomac.2024.133567.

[12] Bößl F, Menzel VC, Chatzisymeon E, Comyn TP, Cowin P, Cobley AJ, Tudela I (2023) Effect of frequency and power on the piezocatalytic and sonochemical degradation of dyes in water. Chem Eng J Adv 14:100477. https://doi.org/10.1016/j.ceja.2023.100477.

[13] Shokoofehpoor F, Mousavi SH, Mohammadi A, Zanjanchi MA (2020) γ-CD-functionalized TiO_2 nanoparticles for the photocatalytic degradation of organic dyes. Prog Color Color Coat 13:23–39. https://doi.org/10.30509/pccc.2020.81593.

[14] Chowdhury P, Viraraghavan T (2009) Sonochemical degradation of chlorinated organic compounds, phenolic compounds and organic dyes–a review. Sci Total Environ 407:2474-2492. https://doi.org/10.1016/j.scitotenv.2008.12.031.

[15] Li Y, Wang T, Zhang S, Zhang Y, Yu L, Liu R (2021) Adsorption and electrochemical behavior investigation of methyl blue onto magnetic nickel-magnesium ferrites prepared via the rapid combustion process. J Alloys Compd 885:160969. https://doi.org/10.1016/j.jallcom.2021.160969.

Mousavi SH, Sohrabnezhad S, Moafi HF (2025) Egg Shell Modified with β-Cyclodextrin, as Green Adsorbent for Dyes from Synthetic Wastewater. Int J Environ Res 19:50. https://doi.org/10.1007/s41742-024-00725-z.

[17] Mousavi SH, Mohammadi A (2018) A cyclodextrin/glycine-functionalized TiO_2 nanoadsorbent: Synthesis, characterization and application for the removal of organic pollutants from water and real textile wastewater. Process Saf Environ Prot 114:1–15. https://doi.org/10.1016/j.psep.2017.12.004.

[18] Mousavi SH, Shokoofehpoor F, Mohammadi A (2019) Synthesis and characterization of γ-CD-modified TiO_2 nanoparticles and its adsorption performance for different types of organic dyes. J Chem Eng Data 64:135–149. https://doi.org/10.1021/acs.jced.8b00656.

[19] Namasivayam C, Kanchana N (1992) Waste banana pith as adsorbent for color removal from wastewaters. Chemosphere 25:1691–1705. https://doi.org/10.1016/0045-6535(92)90316-J.

[20] Yu B, Zhang Y, Shukla A, Shukla SS, Dorris KL (2001) The removal of heavy metals from aqueous solutions by sawdust adsorption—removal of lead and comparison of its adsorption with copper. J Hazard Mater 84:83–94. https://doi.org/10.1016/S0304-3894(01)00198-4.

[21] Mishra SP, Tiwari D, Dubey RS (1997) The uptake behaviour of rice (Jaya) husk in the removal of Zn (II) ions—A radiotracer study. Appl Radiat Isot 48:877–882. https://doi.org/10.1016/S0969-8043(97)00340-0.

[22] Al-Asheh S, Duvnjak Z (1997) Sorption of cadmium and other heavy metals by pine bark. J Hazard Mater 56:35–51. https://doi.org/10.1016/S0304-3894(97)00040-X.

[23] Marshall WE, Johns MM (1996) Agricultural by-products as metal adsorbents: Sorption properties and resistance to mechanical abrasion. J Chem Technol Biotechnol 66:192–198. https://doi.org/10.1002/(SICI)1097-4660(199606)66:2<192::AID-JCTB489>3.0.CO;2-C.

[24] Wafwoyo W, Seo CW, Marshall WE (1999) Utilization of peanut shells as adsorbents for selected metals. J Chem Technol Biotechnol 74:1117–1121. https://doi.org/10.1002/(SICI)1097-4660(199911)74:11<1117::AID-JCTB151>3.0.CO;2-R.

[25] Rodríguez G, Lama A, Rodríguez R, Jiménez A, Guillén R, Fernández-Bolaños J (2008) Olive stone an attractive source of bioactive and valuable compounds. Bioresour Technol 99:5261–5269. https://doi.org/10.1016/j.biortech.2007.11.027.

[26] Namasivayam C, Muniasamy N, Gayatri K, Rani M, Ranganathan K (1996) Removal of dyes from aqueous solutions by cellulosic waste orange peel. Bioresour Technol 54:37–43. https://doi.org/10.1016/0960-8524(96)00044-2.

[27] Hameed BH, Salman JM, Ahmad AL (2009) Adsorption isotherm and kinetic modeling of 2,4-D pesticide on activated carbon derived from date stones. J Hazard Mater 163:121–126. https://doi.org/10.1016/j.jhazmat.2008.06.069.

[28] Toles CA, Marshall WE, Wartelle LH, McAloon A (2000) Steam-or carbon dioxide-activated carbons from almond shells: physical, chemical and adsorptive properties and estimated cost of production. Bioresour Technol 75:197–203. https://doi.org/10.1016/S0960-8524(00)00058-4.

[29] Ahmad A, Khatoon A, Mohd-Setapar SH, Kumar R, Rafatullah M (2016) Chemically oxidized pineapple fruit peel for the biosorption of heavy metals from aqueous solutions. Desalin Water Treat 57:6432–6442. https://doi.org/10.1080/19443994.2015.1005150.

[30] Yu X, Tong S, Ge M, Wu L, Zuo J, Cao C, Song W (2013) Adsorption of heavy metal ions from aqueous solution by carboxylated cellulose nanocrystals. J Environ Sci 25:933–943. https://doi.org/10.1016/S1001-0742(12)60145-4.

[31] Pavan FA, Lima EC, Dias SL, Mazzocato AC (2008) Methylene blue biosorption from aqueous solutions by yellow passion fruit waste. J Hazard Mater 150:703–712. https://doi.org/10.1016/j.jhazmat.2007.05.023.

[32] FENG NC, GUO XY (2012) Characterization of adsorptive capacity and mechanisms on adsorption of copper, lead and zinc by modified orange peel. Trans Nonferrous Met Soc China 22:1224–1231. https://doi.org/10.1016/S1003-6326(11)61309-5.

[33] Boonamnuayvitaya V, Sae-ung S, Tanthapanichakoon W (2005) Preparation of activated carbons from coffee residue for the adsorption of formaldehyde. Sep Purif Technol 42:159–168. https://doi.org/10.1016/j.seppur.2004.07.007.

[34] Shen W, Li Z, Liu Y (2008) Surface chemical functional groups modification of porous carbon. Recent Pat Chem Eng 1:27–40. https://doi.org/10.2174/2211334710801010027.

[35] Karaçetin G, Sivrikaya S, Imamoğlu M (2014) Adsorption of methylene blue from aqueous solutions by activated carbon prepared from hazelnut husk using zinc chloride. J Anal Appl Pyrolysis 110:270–276. https://doi.org/10.1016/j.jaap.2014.09.006.

[36] Demirbas E, Dizge N, Sulak MT, Kobya M (2009) Adsorption kinetics and equilibrium of copper from aqueous solutions using hazelnut shell activated carbon. Chem Eng J 148:480–487. https://doi.org/10.1016/j.cej.2008.09.027.

[37] Crini G, Peindy HN, Gimbert F, Robert C (2007) Removal of CI Basic Green 4 (Malachite Green) from aqueous solutions by adsorption using cyclodextrin-based adsorbent: Kinetic and equilibrium studies. Sep Purif Technol 53:97–110. https://doi.org/10.1016/j.seppur.2006.06.018.

[38] Pal S, Ghorai S, Das C, Samrat S, Ghosh A, Panda AB (2012) Carboxymethyl tamarind-g-poly (acrylamide)/silica: a high performance hybrid nanocomposite for adsorption of methylene blue dye. Ind Eng Chem Res 51:15546–15556. https://doi.org/10.1021/ie301134a.

[39] Paulino AT, Guilherme MR, Reis AV, Campese GM, Muniz EC, Nozaki J (2006) Removal of methylene blue dye from an aqueous media using superabsorbent hydrogel supported on modified polysaccharide. J Colloid Interface Sci 301:55–62. https://doi.org/10.1016/j.jcis.2006.04.036.

[40] Ho YS, McKay G (1999) Pseudo-second order model for sorption processes. Process Biochem. 34:451–465. https://doi.org/10.1016/S0032-9592(98)00112-5.

[41] Cheung CW, Porter JF, Mckay G (2001) Sorption kinetic analysis for the removal of cadmium ions from effluents using bone char. Water Res 35:605–612. https://doi.org/10.1016/S0043-1354(00)00306-7.

[42] Weber Jr WJ, Morris JC (1964) Equilibria and capacities for adsorption on carbon. J Sanit Eng Div 90:79–108. https://doi.org/10.1061/JSEDAI.0000496.

[43] Ncibi MC, Mahjoub B, Seffen M (2007) Kinetic and equilibrium studies of methylene blue biosorption by Posidonia oceanica (L.) fibres. J Hazard Mater 139:280–285. https://doi.org/10.1016/j.jhazmat.2006.06.029.

[44] Mittal A, Mittal J, Malviya A, Kaur D, Gupta VK (2010) Adsorption of hazardous dye crystal violet from wastewater by waste materials. J Colloid Interface Sci 343:463–473. https://doi.org/10.1016/j.jcis.2009.11.060.

[45] Langmuir I (1916) The constitution and fundamental properties of solids and liquids. Part I. Solids. J Am Chem Soc 38:2221–2295. https://doi.org/10.1021/ja02268a002.

[46] Mckay G, El Geundi M, Nassar MM (1987) Equilibrium studies during the removal of dyestuffs from aqueous solutions using bagasse pith. Water Res 21:1513–1520. https://doi.org/10.1016/0043-1354(87)90135-7.

[47] Freundlich, H (1907) Uber die adsorption in losungen. Z Phys Chem 57:385–470. https://doi.org/10.1515/zpch-1907-5723.

[48] Temkin MJ, Pyzhev V (1940) Recent modifications to Langmuir isotherms. Acta Physiochim. 12:217–222.

[49] Mohammadi A, Veisi P (2018) High adsorption performance of β-cyclodextrin-functionalized multi-walled carbon nanotubes for the removal of organic dyes from water and industrial wastewater. J Environ Chem Eng 6:4634–4643. https://doi.org/10.1016/j.jece.2018.07.002.

[50] Quansah JO, Hlaing T, Lyonga FN, Kyi PP, Hong SH, Lee CG, Park SJ (2020) Nascent rice husk as an adsorbent for removing cationic dyes from textile wastewater. Appl Sci 10:3437–3453. https://doi.org/10.3390/app10103437.

[51] Hussain D, Khan SA, Khan TA (2021) Fabrication and characterization of mesoporous guar gum/$NiWO_4$ nanocomposite for efficient adsorption of phloxine B and crystal violet from aqueous solution and evaluation of its antioxidant activity. Colloid Interface Sci Commun 44:100488. https://doi.org/10.1016/j.colcom.2021.100488.

[52] El Naeem GA, Abd-Elhamid AI, Farahat OO, El-Bardan AA, Soliman HM, Nayl AA (2022) Adsorption of crystal violet and methylene blue dyes using a cellulose-based adsorbent from sugercane bagasse: characterization, kinetic and isotherm studies. J Mater Res Technol 19:3241–3254. https://doi.org/10.1016/j.jmrt.2022.06.045.

[53] Takabi AS, Shirani M, Semnani A (2021) Apple stem as a high performance cellulose based biosorbent for low cost and eco-friendly adsorption of crystal violet from aqueous solutions using experimental design: Mechanism, kinetic and thermodynamics. Environ Technol Innovation 24:101947. https://doi.org/10.1016/j.eti.2021.101947.

[54] Chen H, Liu T, Meng Y, Cheng Y, Lu J, Wang H (2020) Novel graphene oxide/aminated lignin aerogels for enhanced adsorption of malachite green in wastewater. Colloids Surf A 603:125281. https://doi.org/10.1016/j.colsurfa.2020.125281.

[55] Sadiq AC, Rahim NY, Suah FB (2020) Adsorption and desorption of malachite green by using chitosan-deep eutectic solvents beads. Int J Biol Macromol 16:3965–3973. https://doi.org/10.1016/j.ijbiomac.2020.09.029.

[56] Jabar JM, Odusote YA (2021) Utilization of prepared activated biochar from water lily (Nymphaea lotus) stem for adsorption of malachite green dye from aqueous solution. Biomass Convers Biorefin 14:5999–6010. https://doi.org/10.1007/s13399-021-01399-9.

[57] Vigneshwaran S, Sirajudheen P, Karthikeyan P, Meenakshi S (2021) Fabrication of sulfur-doped biochar derived from tapioca peel waste with superior adsorption performance for the removal of Malachite green and Rhodamine B dyes. Surf Interfaces 23:100920. https://doi.org/10.1016/j.surfin.2020.100920.

[58] Uddin MK, Nasar A (2020) Walnut shell powder as a low-cost adsorbent for methylene blue dye: isotherm, kinetics, thermodynamic, desorption and response surface methodology examinations. Sci Rep 10:7983. https://doi.org/10.1038/s41598-020-64745-3.

[59] Ifguis O, Ziat Y, Ammou F, Bouhdadi R, Mbarki M, Benchagra M (2022) Theorithecal and experimental study on the thermodynamic parameters and adsorption of methylene blue on “Argania shells” in industrial waters. S Afr J Chem Eng 41:211–222. https://doi.org/10.1016/j.sajce.2022.06.010.

[60] Qiu T, Zeng Y, Ye C, Tian H (2012) Adsorption thermodynamics and kinetics of p-xylene on activated carbon. J Chem Eng Data 57:1551–1556. https://doi.org/10.1021/je300138a.

[61] Xiaodong R, Zhenhu X (2013) Adsorption behavior of three nitroimidazoles in aqueous solutions to magnetic-modified multi-walled carbon nanotubes. Acta Chim Sin 71:625–633. https://doi.org/10.6023/A12110910.

Supplementary Files

This is a list of supplementary files associated with this preprint. Click to download.

- SupplementaryInformation.docx